Scalar variances: LES against measurements and mesh optimization criterion; scalar gradient: a three-dimensional estimation from planar measurements using DNS

By G. Lodato†, P. Domingo†, L. Vervisch† AND D. Veynante‡

Large-eddy simulation (LES) provides space-filtered quantities to compare with measurements, which may have been obtained using a different filtering operation; hence, numerical and experimental results can be examined side-by-side in a time-averaged statistical sense only. Instantaneous, space-filtered and statistically time-averaged signals feature different characteristic length scales, which can be combined in dimensionless ratios. From a manufactured turbulent flame solution, the critical values of these ratios under which measured and computed variances (resolved plus subgrid scale) can be compared without resorting to additional residual terms are first determined. Then, it is shown that the difference in filter sizes imposes the knowledge of the magnitude of the scalar gradient, to accurately compare LES results against measurements. In premixed turbulent flames, scalar gradients are usually obtained from two-dimensional planar experimental diagnostics, for instance when measuring flame surface density. A transformation to evaluate three-dimensional flame surface density from two-dimensional measurements is discussed and evaluated from direct numerical simulation (DNS) of round and planar premixed jet flames.

1. Introduction

Scalar variances are widely used in large-eddy simulation (LES) of turbulent combustion (Pitsch 2006). These variances appear under different forms, time-averaged, filtered, resolved or at the subgrid scale level. Typically, a scalar signal (*e.g.* species mass fraction, enthalpy, temperature) is denoted $\varphi(\underline{x},t)$ and $\langle\varphi\rangle(\underline{x})$ is the time average of this signal:

$$\langle\varphi\rangle(\underline{x}) = \lim_{T\to\infty}\frac{1}{T}\int_0^T \varphi(\underline{x},t)dt \tag{1.1}$$

and $\overline{\varphi}(\underline{x},t)$ is the space filtered average:

$$\overline{\varphi}(\underline{x},t) = \int_{-\infty}^{+\infty} \varphi(\underline{x}',t)\mathcal{G}_\Delta(\underline{x}-\underline{x}')dx' \tag{1.2}$$

where $\mathcal{G}_\Delta$ is a space filter of characteristic scale Δ. Mass weighted filtered and time averaged quantities are also defined from these operators as: $\{\varphi\} = \langle\rho\varphi\rangle / \langle\rho\rangle$ and $\widetilde{\varphi} =$

† LMFN, CORIA - CNRS, Institut National des Sciences Appliquées de Rouen, France
‡ EM2C - CNRS, Ecole Centrale Paris, France

$\overline{\rho\varphi}/\overline{\rho}$. The three signals $\varphi(\underline{x},t)$, $\{\varphi\}(\underline{x})$ and $\widetilde{\varphi}(\underline{x},t)$ have three characteristic thicknesses and length scales δ_L, δ_T and δ_Δ, respectively. In LES, $\delta_L < \delta_\Delta \approx \Delta < \delta_T$.

From their definitions, filtering and averaging operators commute; then whatever above length scales $\overline{\langle\varphi\rangle} = \langle\overline{\varphi}\rangle$. Moreover, for $\Delta << \delta_T$ the time averaged signal does not evolve much at the LES scales and $\langle\varphi\rangle$ is left unchanged by the filtering operation: $\overline{\langle\varphi\rangle} \approx \langle\varphi\rangle$. Combining the commutation of operators and the condition $\Delta << \delta_T$, the relation $\langle\varphi\rangle \approx \langle\overline{\varphi}\rangle$ is obtained (Veynante & Knikker 2006). This paper discusses the interplay between these relations and scalar variance measurements, along with implications regarding the estimation of 3-D flame surface density from 2-D measurements.

2. Variance decomposition: Resolved, subgrid scale (SGS) and residual parts

2.1. *Definitions*

In LES of real combustion systems (Boileau *et al.* 2008), the asymptotic condition $\Delta << \delta_T$ is not always verified and non-negligible residual terms r_ρ, $r_{\rho\varphi}$ and $r_{\rho\varphi^2}$ appear which may be defined so that:

$$\langle\rho\rangle = \langle\overline{\rho}\rangle + r_\rho \tag{2.1}$$

$$\langle\rho\varphi\rangle = \langle\overline{\rho}\widetilde{\varphi}\rangle + r_{\rho\varphi} \tag{2.2}$$

$$\left\langle\rho\varphi^2\right\rangle = \left\langle\overline{\rho}\widetilde{\varphi^2}\right\rangle + r_{\rho\varphi^2} \tag{2.3}$$

then, φ_v, the time-averaged variance may be written:

$$\varphi_v = \left\{\varphi^2\right\} - \{\varphi\}^2 = \frac{\left\langle\overline{\rho}\widetilde{\varphi^2}\right\rangle}{\langle\overline{\rho}\rangle} - \left(\frac{\langle\overline{\rho}\widetilde{\varphi}\rangle}{\langle\overline{\rho}\rangle}\right)^2 + R_{\overline{\rho\varphi^2}} - R_{\overline{\rho\varphi}} \tag{2.4}$$

with

$$R_{\overline{\rho\varphi^2}} = \frac{\langle\overline{\rho}\rangle\, r_{\rho\varphi^2} - \left\langle\overline{\rho\varphi^2}\right\rangle r_\rho}{\langle\overline{\rho}\rangle\left(\langle\overline{\rho}\rangle + r_\rho\right)} \;;\; R_{\overline{\rho\varphi}} = \frac{\langle\overline{\rho}\rangle^2 r_{\rho\varphi}(r_{\rho\varphi} + 2\langle\overline{\rho\varphi}\rangle) - \langle\overline{\rho\varphi}\rangle^2 r_\rho(r_\rho + 2\langle\overline{\rho}\rangle)}{\langle\overline{\rho}\rangle^2\left(\langle\overline{\rho}\rangle^2 + r_\rho^2 + 2\langle\overline{\rho}\rangle r_\rho\right)} \tag{2.5}$$

Introducing $\left\langle\overline{\rho}\widetilde{\varphi}^2\right\rangle$ into Eq. (2.4) leads to:

$$\varphi_v = \left\{\varphi^2\right\} - \{\varphi\}^2 = \underbrace{\frac{\left\langle\overline{\rho}\widetilde{\varphi}^2\right\rangle}{\langle\overline{\rho}\rangle} - \left(\frac{\langle\overline{\rho}\widetilde{\varphi}\rangle}{\langle\overline{\rho}\rangle}\right)^2}_{T_R\text{: Resolved part}} + \overbrace{\frac{\left\langle\overline{\rho}(\widetilde{\varphi^2} - \widetilde{\varphi}^2)\right\rangle}{\langle\overline{\rho}\rangle}}^{T_{SGS}\text{: SGS part}} + R_v \tag{2.6}$$

This last relation provides the exact decomposition of the total variance φ_v into T_R and T_{SGS}, resolved and SGS parts, with an additional residual term $R_v = R_{\overline{\rho\varphi^2}} - R_{\overline{\rho\varphi}}$. T_R is the variance of the filtered field and T_{SGS} the mean of the SGS variance. The constant density case is easily recovered by setting $r_\rho = 0$ and $\rho = cst$ in the above equations.

LES meshes and filters are so that $\Delta = \alpha\delta_L = \beta\delta_T$ with $\alpha > 1$ and $\beta < 1$. The SGS part decreases when $\alpha \to 1$ and would vanish when $\alpha < 1$, as in DNS. The resolved part is negligible when $\beta \to 1$, while the contribution of the residual term R_v decreases with β. For a given reactive front, for $\beta > \beta_R$, the residual term R_v cannot be expected to be small compared to other contributions, where β_R is a critical value to be determined. When comparing LES variances obtained from their resolved and SGS parts, the mesh

must therefore verify $\beta = \Delta/\delta_T < \beta_R$, which also implies $\alpha = (\Delta/\delta_L) < \beta_R(\delta_T/\delta_L)$. The value of β_R is now evaluated for a premixed turbulent flame brush in the flamelet regime.

2.2. *Manufactured premixed flame solution and LES meshes optimization*

Obviously, the analysis of the three terms entering Eq. (2.6) can be performed only in turbulent flame solutions where a sufficiently large number of scales is present. With actual computer capabilities, DNS does not offer the possibility of covering a sufficiently large range of scales to fully investigate these energy-budget questions; a manufactured solution is therefore needed. A synthetic turbulent field is thus manufactured from a large number of laminar flamelets of thickness δ_L, which are randomly distributed to build a mean flame brush. Typically, this solution mimics DNS performed in the flamelet regime; flamelet profiles are transported by turbulence without modification of their internal structure.

The instantaneous progress variable is defined as:

$$c(x,t) = F_L(x - x_L(t)) \tag{2.7}$$

$$x_L(t) = x_o + \xi(t)\kappa(t)\delta_T \tag{2.8}$$

where $F_L(x)$ is the single flamelet distribution obtained from the solution of a methane-air stoichiometric premixed flame computed with detailed GRI chemistry (Smith *et al.* 1999). The progress variable ($c = 0$ in fresh gases and $c = 1$ in fully burnt products) is defined from $Y_c = Y_{CO} + Y_{CO_2}$, normalized by its value in equilibrium products. x_o is the position of the mean flame brush, $x_L(t)$ the position of the flamelet within the turbulent flame brush at time t, $\xi(t)$ is a uniformly distributed random number taking the values ± 1 and $\kappa(t)$ a random Gaussian distribution. The average progress variable profiles of the manufactured solution may be written:

$$\langle c \rangle (x) = \int_{-\infty}^{x} \overline{P}(x_L^*) dx_L^* \tag{2.9}$$

with $\overline{P}(x_L^*)$ the probability density function (pdf) of the flamelets positions. The manufactured solution is operated over a duration $t = T$, so that $\overline{P}(x_L^*)$ is statistically converged.

The terms of Eq. (2.6) extracted from $c(x,t)$ for various values of α and β are displayed in Fig. 1. As expected, T_R, the resolved part decreases when $\beta = \Delta/\delta_T$ increases, while the SGS contribution, T_{SGS}, becomes greater; the decay of T_R versus β is almost linear. The budget $(T_R + T_{SGS})/c_v$ does not sum to unity, untill the always-negative residual part R_v/c_v is added. The sensitivity to $\alpha = \Delta/\delta_L$ is weak for $\beta < 0.2$ and stays moderate for T_{SGS}. For a given β, the resolved part (resp. the SGS part) decreases (resp. increases) when α increases. For a scalar variance budget closed at 1% with the addition of resolved and SGS parts ($R_v/c_v < 0.01$), then β must respect $\beta < \beta_R \approx 0.06$ (Fig. 1), corresponding to $\delta_T/\Delta > 16$.

In LES of a reactive front of characteristic size δ_L, the scalar energy budget can then be completed without resorting to additional residual terms for

$$\alpha_R = \Delta/\delta_L < \beta_R(\delta_T/\delta_L) \ . \tag{2.10}$$

In a typical premixed swirling flow burner (Galpin *et al.* 2008), $\delta_T \approx 0.01$ m and $\delta_L \approx 0.1$ mm, leading to $\alpha_R \approx 6$. This criterion can be used to optimize LES meshes; after a first

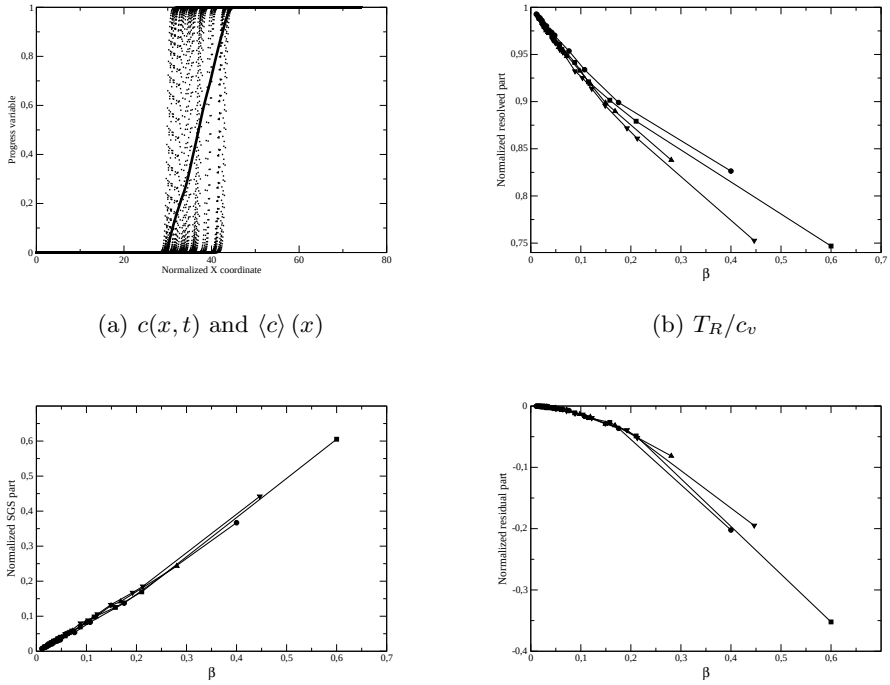

(a) $c(x,t)$ and $\langle c\rangle(x)$ (b) T_R/c_v

(c) T_{SGS}/c_v (d) R_v/c_v

FIGURE 1. (a) - dots: $c(x,t)$ given by Eq. (2.7) for $\delta_T/\delta_L = \alpha/\beta = 12$; line: $\langle c\rangle(x)$. (b) - (c) - (d): Normalized three terms of Eq. (2.6) vs $\beta = \Delta/\delta_T$, normalization is done using c_v. Line with Circle: $\alpha = \Delta/\delta_L = 2$; Square: $\alpha = 3$; Triangle up: $\alpha = 4$; Triangle down: $\alpha = 5$.

simulation performed on a given mesh to estimate δ_T, the grid can be refined at locations where the criterion defined by Eq. (2.10) is not fulfilled.

2.3. *Scaling of SGS variance*

The SGS variance is usually approximated from mixing modeling closures, mostly derived for non-reactive scalars (Pierce & Moin 2004, Domingo *et al.* 2005), under a production-dissipation hypothesis:

$$T_{SGS} = \frac{\left\langle \overline{\rho}(\widetilde{c^2} - \widetilde{c}^2)\right\rangle}{\langle\overline{\rho}\rangle} \propto \frac{\left\langle \overline{\rho}\left(\Delta|\nabla\widetilde{c}|\right)^2\right\rangle}{\langle\overline{\rho}\rangle} \quad . \tag{2.11}$$

Another approach may be followed (Veynante & Knikker 2006) where the flame is supposed as infinitely thin:

$$T_{SGS} \propto \frac{\langle\overline{\rho}\widetilde{c}(1-\widetilde{c})\rangle}{\langle\overline{\rho}\rangle} \quad \text{and} \quad \frac{\langle\overline{\rho}|\nabla\widetilde{c}|\rangle}{\langle\overline{\rho}\rangle} \propto \frac{\langle\overline{\rho}\widetilde{c}(1-\widetilde{c})\rangle}{\Delta\,\langle\overline{\rho}\rangle} \tag{2.12}$$

leading to:

$$T_{SGS} \propto \frac{\langle\overline{\rho}\Delta|\nabla\widetilde{c}|\rangle}{\langle\overline{\rho}\rangle} \quad . \tag{2.13}$$

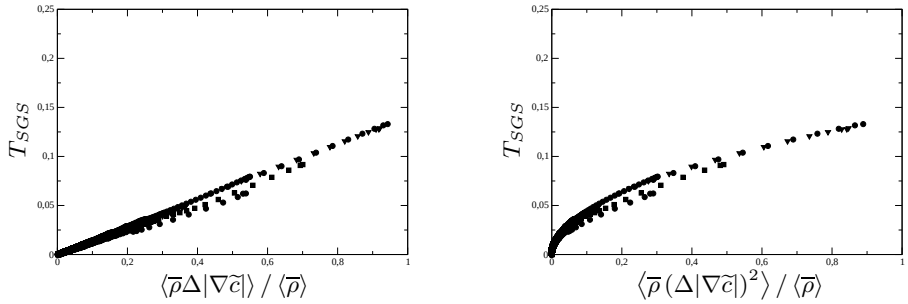

FIGURE 2. T_{SGS} Eq. (2.6) vs (a): $\langle\overline{\rho}\Delta|\nabla\widetilde{c}|\rangle\,/\,\langle\overline{\rho}\rangle$; (b): $\langle\overline{\rho}\,(\Delta|\nabla\widetilde{c}|)^2\rangle\,/\,\langle\overline{\rho}\rangle$. Circle: $\alpha=\Delta/\delta_L=2$; Square: $\alpha=3$, Triangle up: $\alpha=4$; Triangle down: $\alpha=5$.

Analyzing local flame front measurements to estimate SGS variances, Veynante & Knikker (2006) found that the best approximation of the SGS variance was obtained with the linear correlation (Eq. (2.13)). Figure 2(a) shows that the manufactured solution reproduces this result, T_{SGS} scales linearly with the filter size and with the gradient of the filtered field, but not with the square of these quantities. For $\beta > \beta_R$, no scaling was found when the residual term R_v is added to the SGS variance.

Scalar measurements, for instance using Raman or PLIF, are obtained from filtering at a level Δ_*, which may differ from the LES filter Δ. The total variance (lhs of Eq. (2.6)) is decomposed for both filters into resolved and SGS parts; using Eq. (2.13), the resolved parts are related according to:

$$\underbrace{\frac{\langle\overline{\rho}_*\widetilde{\varphi}_*^2\rangle}{\langle\overline{\rho}_*\rangle}-\left(\frac{\langle\overline{\rho}_*\widetilde{\varphi}_*\rangle}{\langle\overline{\rho}_*\rangle}\right)^2}_{\text{Measured}}=\underbrace{\frac{\langle\overline{\rho}\widetilde{\varphi}^2\rangle}{\langle\overline{\rho}\rangle}-\left(\frac{\langle\overline{\rho}\widetilde{\varphi}\rangle}{\langle\overline{\rho}\rangle}\right)^2}_{\text{LES}}+C_v\left(1-\frac{\Delta_*}{\Delta}\frac{\langle\overline{\rho}_*|\nabla\widetilde{\varphi}_*|\rangle\,/\,\langle\overline{\rho}_*\rangle}{\langle\overline{\rho}|\nabla\widetilde{\varphi}|\rangle\,/\,\langle\overline{\rho}\rangle}\right) \tag{2.14}$$

where the subscript $_*$ indicates measured quantities. This last relation suggests that the knowledge of the gradient is useful when comparing measured and LES variances.

3. Evaluation of 3-D scalar gradients and flame surface density from 2-D measurements

3.1. *Background*

In premixed turbulent combustion, the gradient of $c(\underline{x},t)$, the progress variable, is directly related to the flame surface density $\Sigma(c^*;\underline{x},t)=\left(\overline{|\nabla c||c^*}\right)\overline{P}(c^*;\underline{x},t)$, where $\overline{P}(c^*;\underline{x},t)$ is the probability density function of c and $\left(\overline{|\nabla c||c^*}\right)$ the conditional mean value of the gradient for $c=c^*$, the c-value used to locate the flame surface (Pope 1989; Vervisch *et al.* 1995). Integrating overall surfaces leads to (Veynante & Vervisch 2002):

$$\int_0^1\Sigma(c^*;\underline{x},t)dc^*=\int_0^1\left(\overline{|\nabla c||c^*}\right)\overline{P}(c^*;\underline{x},t)dc^*=\overline{|\nabla c|}=\Xi|\nabla\overline{c}| \tag{3.1}$$

with Ξ the wrinkling factor of the turbulent flame; therefore the knowledge of the flame surface also provides information on gradients, useful in Eq. (2.14).

Flame surface density Σ measures the available flame surface per unit volume and its modeling is one of the key approaches to express reaction rates in RANS or LES (Poinsot & Veynante 2005). The mean (or filtered) reaction rate of a species k is written: $\overline{\dot{\omega}}_k = \langle \dot{\Omega}_k \rangle_s \Sigma$, where $\langle \dot{\Omega}_k \rangle_s$ is the surface averaged reaction rate of the k-species per unit of flame area, generally estimated from laminar flame studies under flamelet assumptions. The flame surface density may be determined either from algebraic expressions (Bray *et al.* 1989; Boger *et al.* 1998) or by solving a balance equation (Veynante & Vervisch 2002; Hawkes & Cant 2000). Unfortunately, well-resolved instantaneous flame front 3-D visualizations are not yet available and the experimental determination of flame surface densities, either from planar laser tomography (Veynante *et al.* 1996; Lachaux *et al.* 2005) or planar laser-induced fluorescence measurements (Knikker *et al.* 2002), requires the assumption of a 2-D instantaneous flow (*e.g.* the instantaneous flame front is not wrinkled in the direction normal to the measuring plane).

The objective of this section is to investigate, from DNS, the uncertainties linked to this assumption and to explore whether the actual flame surface density Σ may be inferred from 2-D measurements. Note that similar attempts have been conducted to determine scalar dissipation rate distributions from two-dimensional measurements (Dahm & Buch 1989; Hawkes *et al.* 2009). However, the approach proposed here is quite different as we do not attempt to directly estimate the flame surface density distribution.

3.2. *DNS of a Bunsen flame*

DNS of a turbulent Bunsen flame was performed using the SiTCom code, a CNRS-CORIA MPI parallelized, fully compressible and explicit Finite Volume flow solver based on cartesian grids. This solver approximates the convective terms resorting to the fourth-order centered skew-symmetric-like scheme (Ducros et al., 2000) and the diffusive terms with a fourth-order centered scheme. Time integration is performed using the third-order Runge-Kutta scheme of Gottlieb & Shu (1998). All the boundary conditions are enforced using the 3D-NSCBC approach (Lodato *et al.*, 2008), which has been modified in order to properly account for the chemical source terms, as discussed below.

Assuming that the equivalence ratio of the mixture is lean (*e.g.* there is an excess of air so that the combustion weakly modifies the oxidizer mass fraction), the progress variable and energy source terms $\dot{\omega}_c$ and $\dot{\omega}_e$ relevant to a single-step chemistry may be written:

$$\dot{\omega}_c = \rho K (1-c) \exp\left(-\frac{T_{\mathrm{Ac}}}{T}\right), \quad \text{and} \quad \dot{\omega}_e = c_p T_0 \left(\frac{\alpha_e}{1-\alpha_e}\right) \dot{\omega}_c, \tag{3.2}$$

where usual notations are adopted; K is the pre-exponential factor, T_{Ac} the activation temperature and $\alpha_e = (T_{\mathrm{b}} - T_0)/T_{\mathrm{b}}$ the heat release parameter, which may be related to T_{Ac} by the Zeldovitch number $\beta_e = \alpha_e T_{\mathrm{Ac}}/T_{\mathrm{b}}$. All the results presented were obtained fixing $\alpha_e = 0.8$ and $\beta_e = 8$.

To better control the behavior of the acoustic-sensitive boundary conditions under the presence of heat release, the chemical source terms are accounted for in the computation of characteristic incoming waves (Yoo & Im, 2007). Source terms, in fact, can be treated in analogy to what is done with transverse terms (in-plane convection and pressure gradient, Lodato *et al.*, 2008). This specific treatment of acoustic boundary conditions allows for the reactive front to cross any boundaries of the computational domain.

Two different flow configurations have been computed: (*a*) a $Re_D = 2000$ round flame and (*b*) a $Re_D = 4500$ slot flame (Re_D computed on the bulk velocity U_{b}). The former

Re_D –	D mm	$L_x \times L_y \times L_z$ –	U_b m/s	η μm	h/η min–max	l_t/D –	S_L m/s	u'/S_L –	l_t/δ_l –	Nodes –	Cores (CPUs)
2000	0.5	$4D \times 2D \times 2D$	63.74	2.2	1.2–6.4	0.04	1.7	11.9	2.1	8.5M	2048
4500	1.0	$3D \times 3D \times 1.3D$	71.71	2.4	1.4–10.8	0.025	1.4	16.4	2.2	91M	4096

TABLE 1. Premixed turbulent flame DNS parameters.

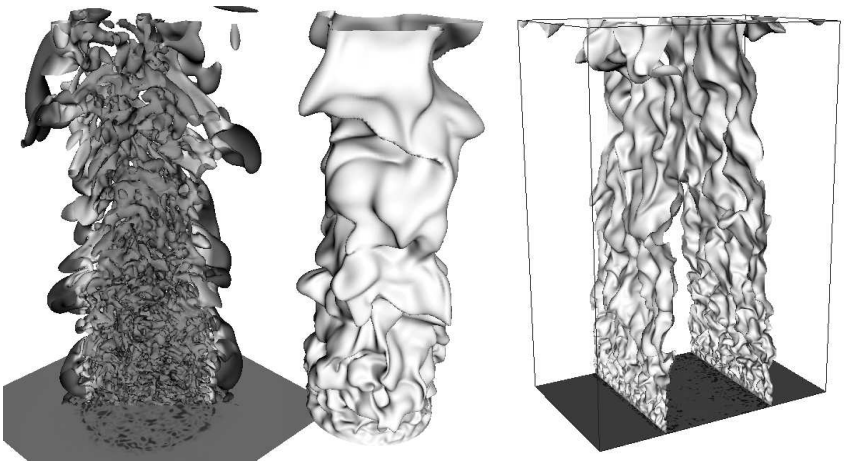

FIGURE 3. Left: $Re_D = 2000$ round jet flame, Q-criterion and flame surface. Right: $Re_D = 4000$ slot burner flame, flame surface.

was computed using subsonic non-reflecting inlet condition and subsonic non-reflecting outflows on all the other five boundaries, the latter had identical boundary types, except in the spanwise direction where periodic conditions were enforced. In both cases, turbulence was promoted by injecting a correlated random noise (Klein *et al.*, 2003) at the inlet, with correlation length l_t and intensity u'.

Grid spacing has been chosen in order to correctly resolve all the relevant scales of turbulence, as well as the flame thickness. With regard to the first point, the Kolmogorov length-scale η has been evaluated from the classical scaling $\eta \sim \ell Re_t^{-3/4}$, $\ell \sim 0.1D$ being an estimation of the integral length-scale, $Re_t \sim u'\ell/\nu$ and $u'^2 \sim 0.1U_\mathrm{b}^2$, estimations checked from results. As can be seen in Table 1, grid spacing h is of the order of η in regions where turbulence develops, and the maximum values are attained far from the shear layers, where velocity fluctuations do not exist.

With regard to the flame resolution, 1-D preliminary tests have revealed that a good estimation of the maximum grid spacing h_max can be obtained from the laminar flame speed S_L and the cinematic viscosity ν as $h_\mathrm{max} \propto 0.3\nu/S_L$. This criterion, actually, fixes the maximum laminar flame speed that can be resolved on a given computational grid; S_L was set accordingly for both simulations. The main parameters for the two DNS are summarized in Table 1.

3.3. *Basic geometrical flame properties*

For clarity, the following derivations are conducted for a statistically 2-D turbulent flame in Cartesian coordinates. The proposed relations are easily recast in terms of cylindrical coordinates, considering a statistically axisymmetrical turbulent flame, as observed in the DNS round-jet flame. Let x denote the downstream direction and (x, y) the measuring plane, for which Mie diffusion or laser-induced fluorescence instantaneous flame front visualizations are available. No measurements are conducted along the transverse direction z. In the following, θ is the angle of the projection, in the measuring plane, of the unit vector $\mathbf{n}$ normal to the instantaneous flame front with the transverse direction y, while ϕ measures the angle between $\mathbf{n}$ and the measuring plane (x, y), as shown in Fig. 4(a). θ is known from measurements and $-\pi \leq \theta \leq +\pi$. For instantaneous flame front parallel to the downstream direction x, $\theta = 0$. The off-measuring plane angle ϕ is unknown and $-\pi/2 \leq \phi \leq +\pi/2$. For instantaneous 2-D flame front, $\phi = 0$.

According to these notations, the unit vector normal to the flame front in the (x, y)-plane and in the 3-D field are respectively:

$$\mathbf{n}_{(x,y)} = (\sin\theta, \cos\theta, 0) \quad \text{and} \quad \mathbf{n} = (\sin\theta\cos\phi, \cos\theta\cos\phi, \sin\phi) \tag{3.3}$$

The density of the isosurface $c = c^*$, Σ, and the corresponding value extracted from 2-D measurements in the (x, y) plane, $\Sigma_{(x,y)}$, are given by Pope (1988):

$$\Sigma = \left(\overline{|\nabla c| \mid c^*}\right) P(c^*) \tag{3.4}$$

$$\Sigma_{(x,y)} = \left(\overline{|\nabla c|_{(x,y)} \mid c^*}\right) P(c^*) \ . \tag{3.5}$$

the subscript (x, y) denotes 2-D measurements in the (x, y)-plane. Then:

$$\Sigma_{(x,y)} = \left(\overline{\cos\phi\,|\nabla c| \mid c^*}\right) P(c^*) = \langle\cos\phi\rangle_s \Sigma \tag{3.6}$$

Two- and three-dimensional flame surface densities are thus linked through $\langle\cos\phi\rangle_s$, the surface averaged value of $\cos\phi$. For $\phi = 0$, both flame surface densities are equal. Two- and three dimensional mean values of the scalar dissipation rate, proportional to $|\nabla c|^2$ are related through mean values of $\cos^2\phi$. Dahm & Buch (1989) and Hawkes *et al.* (2009) then propose to estimate the distribution of the scalar dissipation rate from the probability density function of $\cos^2\phi$; an equivalent approach for flame surface density will be investigated in the future but is not retained here.

Figure 4(b) displays histograms of angles θ and ϕ as extracted from the DNS database. As expected, their mean values are close to zero because of the axi-symmetry of the mean flowfield. They have similar variances, meaning that flame front movements around the y-direction in the plane (x, y) (θ angles) are comparable to off-plane movements (ϕ angles). Also, θ and ϕ are found to be poorly correlated (not shown here) and may be assumed statistically independent.

The vector $\mathbf{n}$ normal to the instantaneous flame front is a unit vector:

$$\langle n_x n_x\rangle_s + \langle n_y n_y\rangle_s + \langle n_z n_z\rangle_s = 1 \ . \tag{3.7}$$

where n_i denotes the component along the i-th direction. Decoupling each component into mean and fluctuation, $n_i = \langle n_i\rangle_s + m_i$, with $\langle m_i\rangle_s = 0$ gives:

$$\langle n_x\rangle_s\langle n_x\rangle_s + \langle m_x m_x\rangle_s + \langle n_y\rangle_s\langle n_y\rangle_s + \langle m_y m_y\rangle_s + \langle n_z\rangle_s\langle n_z\rangle_s + \langle m_z m_z\rangle_s = 1 \tag{3.8}$$

Three additional assumptions are now introduced:

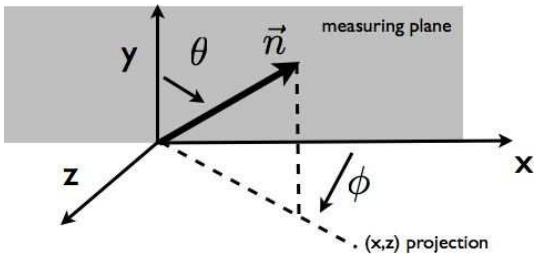

(a)

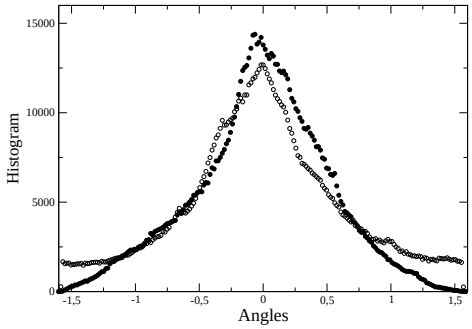

(b)

FIGURE 4. (a): x is the downstream direction, instantaneous flame front visualizations are performed in the (x, y) plane. θ (respectively ϕ) measures the angle of the projection, in the measuring plane, of the unit vector $\mathbf{n}$ normal to the instantaneous flame front with the y-direction (respectively off the measuring plane). (b): Histograms of angles θ (empty circles) and ϕ (filled circles) from DNS (round-jet flame, points in the flame front $0 < c < 1$, $|\nabla c| > 0$).

(a) In mean, the flow is 2-D (or axi-symmetric), hence $\langle n_z \rangle_s = 0$.

(b) According to Eq. (3.3), $n_x = (\cos\phi) n_{x_{(x,y)}}$ and $n_y = (\cos\phi) n_{y_{(x,y)}}$, where $n_{i_{(x,y)}}$ are the components of $\mathbf{n}_{(x,y)}$, the unit vector normal to the flame front in the (x, y)-plane. When angles θ and ϕ are statistically independent, these relations give $\langle n_i \rangle_s \approx \langle \cos\phi \rangle_s \langle n_{i_{(x,y)}} \rangle_s^{2D}$ and suggest the introduction of $\langle m_i m_i \rangle_s \approx \langle \cos\phi \rangle_s^2 \langle m_{i_{(x,y)}} m_{i_{(x,y)}} \rangle_s^{2D}$, where $i = x, y$ and the suffix $2D$ denotes surface averages in the (x, y) plane.

(c) The fluctuations of the normal vector in the z-direction, $\langle m_z m_z \rangle_s$, remain unknown. Assuming similar statistics for θ and ϕ angles provides an estimation of this quantity from the fluctuations of the normal vector in the plane (x, y) around the y-direction:

$$\langle m_z m_z \rangle_s \approx \langle m_y m_y \rangle_s \approx \langle \cos\phi \rangle_s^2 \langle m_{y_{(x,y)}} m_{y_{(x,y)}} \rangle_s^{2D} \tag{3.9}$$

Eq. (3.8) then becomes:

$$\langle \cos\phi \rangle_s^2 \left(1 + \langle m_{y_{(x,y)}} m_{y_{(x,y)}} \rangle_s^{2D} \right) = 1 \tag{3.10}$$

leading to, using Eq. (3.6):

$$\Sigma \approx \left(\sqrt{1 + \langle m_{y_{(x,y)}} m_{y_{(x,y)}} \rangle_s^{2D}} \right) \Sigma_{(x,y)} \tag{3.11}$$

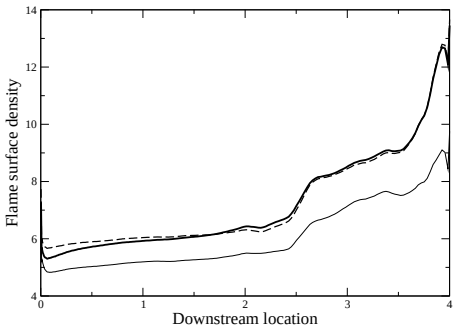

(a)

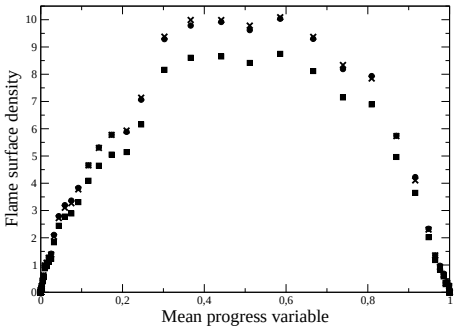

(b)

FIGURE 5. Flame surface by Eq. (3.12). (a): vs x, normalized bunsen flame downstream location. (b): transverse profile vs mean progress variable. Bold line (a) and Circle (b): DNS 3-D-Σ; Thin line (a) and Square (b): 2-D measurements ($\Sigma_{(x,y)}$); dashed line (a) and cross (b): 3-D reconstruction from Eq. (3.11).

providing an estimation of the 3-D flame surface density from 2D measurements performed in the (x, y)-plane.

3.4. *3-D estimation against DNS results*

Relation (3.11) is now investigated from the DNS data. Flame surface densities are extracted identifying the flame front with the isosurface $c^* = 0.88$, corresponding to the maximum value of the reaction rate. To increase the number of samples, all possible (x, y)-planes are considered, *e.g.* 2-D statistics are extracted from all planes containing the burner centerline (x-axis).

Figure 5(a) displays the evolution of the total flame surface along the burner centerline. This total surface depends on the downstream location and is defined as:

$$\Sigma_{tot}(x) = \int_{-\infty}^{+\infty}\int_{-\infty}^{+\infty} \Sigma \, dy \, dz \tag{3.12}$$

Two-dimensional measurements are found to underestimate the flame surface by about 16% while Eq. (3.11) recovers the true value with an error of about 0.3% on the total flame surface. This finding is confirmed in Fig. 5(b), showing transverse profiles of the flame surface density as a function of the progress variable c. Similar results are found with the slot burner configuration (not shown).

4. Conclusion

A manufactured turbulent premixed flame solution has been introduced to discuss a LES mesh criterion based on characteristic laminar flame and mean flame brush thicknesses. The scaling of scalar variance in terms of scalar gradient was also addressed with this synthetic solution and previous experimental observations recovered. The 3-D estimation of this scalar gradient from 2-D measurements was then addressed using both geometrical derivations and DNS results.

Acknowledgments

The authors have benefited from fruitful discussions with CTR Summer Program participants. Computing resources were provided by IDRIS-CNRS (http://www.idris.fr/) and CRIHAN (http://www.crihan.fr/).

REFERENCES

Boger, M., Veynante, D., Boughanem H. & Trouvé A. 1998 Direct numerical simulation analysis of flame surface density concept for large eddy simulation of turbulent premixed combustion. In *Twenty-seventh Symposium (International) on Combustion*, 917–925. Combust. Inst.

Boileau, M., Staffelbach, G., Cuenot, B., Poinsot, T. & Bérat, C. 2008 LES of an ignition sequence in a gas turbine engine. *Combust. Flame* **154**(1/2): 2-22.

Bray, K.N.C., Champion, M. & Libby., P. 1989 The interaction between turbulence and chemistry in premixed turbulent flames. In *Turbulent Reacting Flows*, R. Borghi and S. Murphy (Eds.), Vol. 40 of *Lecture Notes in Engineering*, pp. 541 – 563. Springer.

Dahm, W. & Buch, K. 1989 Lognormality of the scalar dissipation pdf in turbulent flows. *Phys. Fluids A1* **7**, 1290–1293.

Domingo, P., Vervisch, L., Payet, S. & Hauguel, R. 2005 DNS of a premixed turbulent V-flame and LES of a ducted-flame using a FSD-PDF subgrid scale closure with FPI tabulated chemistry, *Combust. Flame* **143**(4) 566–586.

Domingo, P., Vervisch, L. & Veynante, D. 2008 Large-Eddy Simulation of a lifted methane-air jet flame in a vitiated coflow, *Combust. Flame* **153**(3) 415–432.

Ducros, F., Laporte, F., Soulères, T., Guinot, V., Moinat, P. & Caruelle B. 2000 High-order fluxes for conservative skew-symmetric-like schemes in structured meshes: Application to compressible flows. *J. Comput. Phys.* **161**:114–139.

Galpin, J., Naudin, A., Vervisch, L., Angelberger, C., Colin, O. & Domingo, P. 2008 *Combust. Flame* **155**(1):247–266.

Gottlieb, S. & Shu, C. 1998 Total variation diminishing runge-kutta schemes. *Math. Comput.* **67**(221):73–85.

Hawkes, E. & Cant, S. 2000 A flame surface density approach to large eddy simulation of premixed turbulent combustion. *Proc. Combust. Inst.* **28**:51–58.

Hawkes, E., Sankaran, J., Chen, R., Kaiser, S. & Franck, J.2009 Analysis of lower-dimensional approximations to the scalar dissipation rate using direct numerical simulations of plane jet flames. *Proc. Combust. Inst. in press.*

Klein, M., Sadiki, A. & Janicka, J. 2003 A digital filter based generation of inflow data for spatially developing direct numerical or large eddy simulations. *J. Comput. Phys.* **186**:652–665.

Knikker, R., Veynante,D. & Meneveau, C. 2002 A priori testing of a similarity model for large eddy simulations of turbulent premixed combustion. *Proc. Combust. Inst.* **29**:2105–2111.

Lachaux, T., Halter, F., Chauveau, C., Gokalp, I. & Shepherd, I. 2005 Flame front analysis of high-pressure turbulent lean premixed methane–air flames. *Proc. Combust. Inst.* **30**:819–826.

Lodato, G., Domingo, P. & Vervisch, L. 2008 Three-dimensional boundary conditions for direct and large-eddy simulation of compressible viscous flows. *J. Comput. Phys.* **227**(10):5105–5143.

Pierce, C. & Moin, P. 1999 A dynamic model for subgrid-scale variance and dissipation rate. *Phys. Fluids* **10**(12):3041-3044.

Pitsch, H. 2006 Large-Eddy Simulation of turbulent combustion. *Ann. Rev. Fluid Mech.* **38**:453–482.

Poinsot, T. & Veynante, D. 2005 *Theoretical and Numerical Combustion* (Second ed.). Edwards Inc., Philadelphia, Penn.

Pope, S. 1988 The evolution of surfaces in turbulence. *Int. J. Eng. Sci.* **26**(5):445–469.

Smith, G. P. , Golden, D. M., Frenklach, M., Moriarty, N. W., Eiteneer, B., Goldenberg, M., Bowman, C. T., Hanson, R. K., Song, S., Gardiner, W., C., Lissianski, V., V, Qin, Z. 1999 http://www.me.berkeley.edu/gri-mech/.

Tatsumi, S., Martinelli, L. & Jameson, A. 1995 Flux-limited schemes for the compressible navier-stokes equations. *AIAA Journal* **33**(2):252–261.

Vervisch, L., Bidaux, E., Bray, K.N.C. & Kollmann W. 1995 Surface density function in premixed turbulent combustion modeling, similarities between probability density function and flame surface approaches, *Phys. Fluids* **7**(10):2496–2503.

Veynante, D. & Knikker, R.. 2006 Comparison between LES results and experimental data in reacting flows. *J. Turbul.*, 7, DOI: 10.1088/1468-5248/5/1/037.

Veynante, D., Piana, J, Duclos, J. & Martel, C. 1996. Experimental analysis of flame surface density model for premixed turbulent combustion. In *Twenty-sixth Symposium (International) on Combustion*, 413–420. Combust. Inst.

Veynante, D. & Vervisch, L. 2002 Turbulent combustion modeling. *Proc. Energy and Comb. Science* **28**(3):193–301.

Yoo, C. & Im., H. 2007 Characteristic boundary conditions for simulations of compressible reacting flows with multi-dimensional, viscous and reaction effects. *Combust. Theor. Model.*, 11(2):259–286.